

Accelerated Newton-Raphson GRAPE methods for optimal control

David L. Goodwin,^{1,2,*} Pranav Singh,³ Mohammadali Foroozandeh,¹ and Mads Sloth Vinding^{4,†}

¹*Chemistry Research Laboratory, University of Oxford, Mansfield Road, Oxford OX1 3TA, UK*

²*Institute for Biological Interfaces 4 – magnetic resonance,*

Karlsruhe Institute for Technology (KIT), Karlsruhe, Germany

³*Department of Mathematical Sciences, University of Bath, Bath BA2 7AY, UK*

⁴*Center of Functionally Integrative Neuroscience (CFIN),*

Department of Clinical Medicine, Faculty of Health, Aarhus University, Denmark

(Dated: July 21, 2022)

A Hessian based optimal control method is presented in Liouville space to mitigate previously undesirable polynomial scaling of computation time. This new method, an improvement to the state-of-the-art Newton-Raphson GRAPE method, is derived with respect to two exact time-propagator derivative techniques: auxiliary matrix and ESCALADE methods. We observed that compared to the best current implementation of Newton-Raphson GRAPE method, for an ensemble of 2-level systems, with realistic conditions, the new auxiliary matrix and ESCALADE Hessians can be 4-200 and 70-600 times faster, respectively.

PACS numbers: 02.30.Yy, 02.60.Pn, 03.67.-a, 87.80.Lg

Keywords: Optimal Control, Hessian, Newton-Raphson, GRAPE

INTRODUCTION

The problem of transferring the state of a dynamical system to a desired target state while minimising the remaining distance and costs is often solved with optimal control theory [1, 2]. Applications include quantum sensing [3–6], quantum computing [7–9], and nuclear magnetic resonance (NMR) spectroscopy [10–13] and imaging (MRI) [14, 15].

A number of different approaches to optimal control (OC) has lead to the development of different methods: Lagrangian methods [16–19]; minimal time optimal control [10]; gradient ascent pulse engineering (GRAPE) [12]; sophisticated gradient-free searches [20, 21]; Krylov-Newton methods [22]; optimal control with a basis of analytic controls [23, 24]; a tensor product approach for large quantum systems [25]. The method outlined in this work is based on a piecewise-constant control pulse approximation [26–29] of GRAPE [12, 30, 31] using a gradient following numerical optimisation.

Although finding an optimal solution to the problem of controlling a single 2-level system from a defined initial system state to a desired target state, a *state-to-state* problem, is considered straight-forward and computationally inexpensive with modern methods and computing power; an OC problem can become numerically and computationally arduous [32], particularly for applications that account for practical hardware configurations and limitations [11, 33, 34]. Additionally, the computational expense can increase dramatically when optimising over an ensemble of systems, such as the case in solid-state nuclear magnetic resonance [13, 35, 36], where the ensemble also includes crystalline orientations of a powder average [37]. The particular application of OC of interest to the authors is that of a neural network based method for MRI [38–40] and a method of morphic OC [41], requiring hundreds of thousands of optimised pulse shapes to form their optimal libraries.

Keeping the example of MRI, the utility of OC is high-

lighted when considering the legal constraints of power deposition safeguards [42] and the obvious financial rewards of reducing the time a patient stays inside the MRI machine.

Modern techniques can mitigate protracted numerical convergence with a quadratically convergent optimisation method, requiring the calculation of a Hessian matrix, giving a large saving in the number of required serial optimisation iterations [31, 35, 43]. However, it is known within the community that calculation of the Hessian matrix does not scale well to a control problem with a large number of controllable amplitudes [44] (also shown in Fig. 1).

This communication presents a jump in computational efficiency of multiple-orders of magnitude with a rework of the original method, devised to calculate the exact Hessian matrix [31, 35, 45], and the recently published exact, matrix-free, method of efficient spin control using analytical Lie algebraic derivatives (ESCALADE) [43]. The manuscript will present the mathematical formulation of these exact Newton-Raphson GRAPE methods in the irreducible spherical-tensor basis of a Liouville space and show a newly devised method to calculate the Hessian matrix with $\mathcal{O}(N)$ scaling, compared to the previous $\mathcal{O}(N^2)$ scaling (Fig. 1). Results show the comparative speedup of this method to the original in the context of state-to-state MRI problems, requiring a generalisation of the ESCALADE method with calculations of optimal z-controls.

EXACT NEWTON-RAPSON OPTIMAL CONTROL

Optimal control in Liouville space

A quantum system can be described by a density operator, $\hat{\rho}(t)$; a time-dependent system state. The evolution of this state is dictated by the Liouville-von Neumann equation,

$$\frac{\partial}{\partial t} \hat{\rho}(t) = -i[\hat{H}(t), \hat{\rho}(t)] \quad (1)$$

where $\hat{H}(t)$ is a time-dependent Hamiltonian, an operator in a Hilbert space with a spectrum of allowed energy levels. The usual factor of \hbar is dropped here, resulting in the eigenspectrum of \hat{H} expressed in angular frequency units. The methods presented in this manuscript are particular to a Liouville space, also named the adjoint representation[30, 31, 35]. A system state in a Liouville space is represented by a vector, $|\hat{\rho}\rangle$, obtained by stacking columns of the density operator $\hat{\rho}$ with Eq. (1) becoming

$$\frac{\partial}{\partial t}|\hat{\rho}(t)\rangle = -i\hat{L}(t)|\hat{\rho}(t)\rangle, \quad \hat{L}(t) \triangleq \mathbb{1} \otimes \hat{H}(t) - \hat{H}(t)^\dagger \otimes \mathbb{1} \quad (2)$$

where the identity matrix, $\mathbb{1}$, and Hamiltonian have the same dimension.

The form of a bilinear control problem is to split that which is controllable, *the control*, from that which is not, *the drift*. The Liouvillian for a control problem with x-, y-, and z- controls on a 2-level systems can be written as

$$\hat{L}(t) = \underbrace{\omega \hat{L}_z}_{\text{drift}} + \underbrace{c_x(t)\hat{L}_x + c_y(t)\hat{L}_y + c_z(t)\hat{L}_z}_{\text{control}} \quad (3)$$

where the angular frequency ω is the time-independent resonant frequency offset, $c_{x,y,z}(t)$ are time-dependent control amplitudes, and $\hat{L}_{x,y,z}$ are Pauli matrices of a Liouville space.

The OC method of GRAPE [12] uses piecewise constant control pulses, where control pulses are constant over a small time interval, Δt [28, 29]:

$$c_k(t) \rightarrow [c_{k,1} \ c_{k,2} \ \cdots \ c_{k,N}], \quad k \in \{\text{x, y, z}\} \quad (4)$$

using the notation $c_{k,n} \equiv c_k(t_n)$ for convenience, and $t_N = N\Delta t$. This discrete formulation allows numerical solution to Eq. (2), given an initial state of the system $|\hat{\rho}_0\rangle$, through time-ordered propagation

$$|\hat{\rho}_N\rangle = \hat{P}_N \hat{P}_{N-1} \cdots \hat{P}_2 \hat{P}_1 |\hat{\rho}_0\rangle \quad (5)$$

where \hat{P}_n are time-propagators of an isolated time-slice and are defined through the exponential map

$$|\hat{\rho}_n\rangle = \hat{P}_n |\hat{\rho}_{n-1}\rangle, \quad \hat{P}_n = e^{-i\hat{L}_n \Delta t} \quad (6)$$

The matrix exponential of Eq. (6) usually calculated with the Padé approximant, Taylor series, or Krylov propagation [35].

An additional method to calculate the time-propagators of a 2-level system is by explicitly calculating the elements of the matrix. In a spherical-tensor basis, this matrix is the Wigner-matrix [46]:

$$\hat{P}_n = \begin{bmatrix} \alpha^2 & \sqrt{2}\alpha\beta & \beta^2 \\ -\sqrt{2}\alpha\beta^* & \alpha\alpha^* - \beta\beta^* & \sqrt{2}\alpha^*\beta \\ \beta^{*2} & -\sqrt{2}\alpha^*\beta^* & \alpha^{*2} \end{bmatrix} \quad (7)$$

which is formulated in terms of the complex elements

$$\alpha = \cos \phi + i \frac{z}{r} \sin \phi, \quad \beta = \frac{y}{r} \sin \phi + i \frac{x}{r} \sin \phi, \quad (8)$$

where the shorthands $x = c_{x,n}$, $y = c_{y,n}$, and $z = c_{z,n} + \omega$ are used, $\phi = \frac{1}{2}r\Delta t$ is a polar angle of rotation, and $r = \sqrt{x^2 + y^2 + z^2}$ is the polar radius.

As a notational convenience for what follows, the following *effective propagators* are defined as the effect of the pulse between time slices m and n :

$$\mathbf{U}_m^n \triangleq \hat{P}_n \hat{P}_{n-1} \cdots \hat{P}_{m+1} \hat{P}_m, \quad \forall (1 \leq m \leq n \leq N) \quad (9)$$

where a backward (time-reversed) propagation can be denoted by $\mathbf{U}_n^m = \mathbf{U}_m^n$.

Optimal control requires a metric to optimise; the *fidelity* [12, 47], \mathcal{F} , a measure how well the pulses perform a desired control task. The task of the OC problem is to find a set of control amplitudes, $c_{x,y,z}(t)$, that maximise the fidelity e.g. the real part of an inner product:

$$\max_{c_{x,y,z}(t)} (\mathcal{F}) = \max_{c_{x,y,z}(t)} \left(\text{Re} \langle \hat{\sigma} | \mathbf{U}_1^N | \hat{\rho}_0 \rangle \right) \quad (10)$$

This form of the fidelity metric is defined in terms of state-to-state problems, where a system is in a defined initial state, $|\hat{\rho}_0\rangle$, and the control task is to take this state to a desired one, $|\hat{\sigma}\rangle$. With the notation introduced in Eq. (9), \mathbf{U}_1^N is interpreted as the effective propagator over the shaped pulse. In addition to Eq. (5), the system is propagated backwards from the desired target state,

$$|\hat{\chi}_N\rangle = \hat{P}_n^\dagger \hat{P}_{n-1}^\dagger \cdots \hat{P}_{N-1}^\dagger \hat{P}_N^\dagger |\hat{\sigma}\rangle \quad (11)$$

which is termed the *adjoint state* of the control problem [35].

GRAPE is a gradient following numerical optimisation method and requires derivatives of the fidelity with respect to the controls. In turn, this requires the directional propagator derivatives, $D_{k,n}^a$; with the subscripts k denoting the derivative in the direction of \hat{L}_k and n denoting the derivative operating on the time-propagator \hat{P}_n . For each time-slice, n , and for each control direction $\hat{L}_k \in \{\hat{L}_x, \hat{L}_y, \hat{L}_z\}$, the a^{th} order derivative takes the form

$$\nabla^a \mathcal{F}(c_{k,n}) = \text{Re} \langle \hat{\chi}_{n+1} | \underbrace{D_{k,n}^a}_{N \text{ times}} \hat{\rho}_{n-1} \rangle, \quad (12)$$

where bra-ket notation explicitly shows vector structures i.e. $|D_{k,n}^a \hat{\rho}_{n-1}\rangle = D_{k,n}^a |\hat{\rho}_{n-1}\rangle$. The number of forward and backward propagations is indicated for each control channel to produce a gradient vector, $\nabla \mathcal{F}$, or the diagonal elements of a Hessian matrix, $\nabla^2 \mathcal{F}$.

This is sufficient for a fidelity gradient, scaling linearly with N , but a fidelity Hessian also requires mixed second order derivatives [31], where the off-diagonal Hessian elements are

$$\nabla^2 \mathcal{F}(c_{k,n}, c_{j,m}) = \text{Re} \langle \hat{\chi}_{n+1} | \underbrace{D_{k,n}^a}_{N \text{ times}} | \underbrace{\mathbf{U}_{m+1}^{n-1} | D_{j,m} \hat{\rho}_{m-1} \rangle}_{\frac{1}{2}N(N-1) \text{ times}} \rangle \quad (13)$$

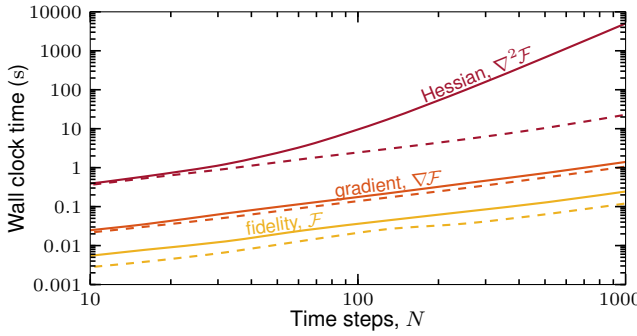


FIG. 1. Average wall-clock time of fidelity, gradient, and Hessian for increasing N . Solid lines show the Newton-Raphson GRAPE method [31] and dashed lines show the proposed *accelerated* Newton-Raphson GRAPE method. Both methods use the auxiliary matrix method [45] to calculate propagator derivatives.

Clearly, the form of Eq. (13) has a central propagator that cannot be absorbed into the bra or ket because it depends on both t_n and t_m , and therefore the computation scales polynomially with $\frac{1}{2}N(N-1)$ (the factor $\frac{1}{2}$ comes from the symmetric property of a Hessian [35]). This is known within the OC community [44] and is highlighted in Fig. 1. The linear plots of the fidelity and gradient, on log-log axes, show these calculations are efficient with increasing N , whereas the Hessian calculation time is not linear on these log-log axes. The subject of this manuscript is to mitigate this undesirable scaling, resulting in a linearly scaling Hessian calculation (dashed lines in Fig. 1), after the following section outlines calculation of directional propagator derivatives.

Directional propagator derivatives with auxiliary matrices

As has been published previously [31, 35, 45], exact propagator derivatives required by Eq. (12) and (13) can be calculated by exponentiating an auxiliary matrix: resulting in an upper triangular block matrix [48] with a time-propagator, \hat{P}_n , on the block diagonal, and with the directional derivative of that propagator, calculated in the direction of a control operator, in the upper triangular block. The first and second order propagator derivatives can be extracted from

$$\exp \begin{bmatrix} \mathbf{A}_n & \mathbf{C}_j & \\ 0 & \mathbf{A}_n & \mathbf{C}_k \\ 0 & 0 & \mathbf{A}_n \end{bmatrix} = \begin{bmatrix} \hat{P}_n & D_{j,n} & \frac{1}{2}D_{jk,n}^2 \\ 0 & \hat{P}_n & D_{k,n} \\ 0 & 0 & \hat{P}_n \end{bmatrix} \quad (14)$$

where the block matrix is formed from $\mathbf{A}_n = -i\hat{L}_n\Delta t$, as in Eq. (6), and $\mathbf{C}_k = -i\hat{L}_k\Delta t$ are functions of the control operators with $j, k \in \{\text{x}, \text{y}, \text{z}\}$.

Directional propagator derivatives with ESCALADE

Whereas Eq. (14) is exact, the matrix exponential is expensive. Foroozandeh and Singh recently devised a method that is free from this expensive matrix exponential calculation, in the OC method of Efficient Spin Control using Analytical Lie Algebraic Derivatives (ESCALADE) [43]. This method can also be extended with interaction propagator splitting [49].

The efficient method of ESCALADE to calculate the directional derivatives in Eqs. (12) and (13), in this single spin model, is to construct a matrix with rows containing all elements needed to construct the propagator derivatives

$$\begin{bmatrix} \Theta_x \\ \Theta_y \\ \Theta_z \end{bmatrix} = \text{vec}[\mathbb{1}] + \frac{\sin^2 \phi}{\phi r} \text{vec}[\mathbf{S}] + \frac{2\phi - \sin 2\phi}{2\phi r^2} \text{vec}[\mathbf{S}^2] \quad (15)$$

where $\text{vec}[\mathbb{1}]$ is a vectorised identity matrix, with a vectorisation operation on a matrix \mathbf{A} such that $\mathbf{A} = \text{vec}^{-1}[\text{vec}[\mathbf{A}]]$. The skew-symmetric matrix \mathbf{S} is

$$\mathbf{S} = \begin{bmatrix} 0 & z & -y \\ -z & 0 & x \\ y & -x & 0 \end{bmatrix} \quad (16)$$

and the symmetric matrix \mathbf{S}^2 is calculated algebraically. In turn, the directional propagator derivatives can be written as

$$D_{k,n} = \hat{P}_n \left[\text{vec}^{-1}[\Sigma \Theta_k] \right] \quad (17)$$

$$D_{jk,n}^2 = \hat{P}_n \left[\text{vec}^{-1}[\Sigma \Theta_{jk}] \right] \quad (18)$$

where $\Sigma = [\text{vec}[\mathbf{C}_x] \text{ vec}[\mathbf{C}_y] \text{ vec}[\mathbf{C}_z]]$ is a 3-column matrix to be multiplied with the 3-row matrix of Θ_k . Using a similar notation to Eq. (15), the Θ_{jk} matrices required by the second order derivatives in Eq. (18) are

$$\begin{bmatrix} \Theta_{jx} \\ \Theta_{jy} \\ \Theta_{jz} \end{bmatrix} = \frac{\cos(2\phi) - 1}{r^2} \text{vec} \left[\mathbf{S} \frac{d\mathbf{S}}{dj} + \frac{d\mathbf{S}}{dj} \mathbf{S} \right] + \frac{2\phi - \sin(2\phi)}{r^3} \text{vec} \left[\frac{d\mathbf{S}}{dj} \right] + \frac{2k(1 - \cos(2\phi) - \phi \sin(2\phi))}{r^3} \text{vec}[\mathbf{S}] + \frac{3k \sin(2\phi) - 2k\phi(2 + \cos(2\phi))}{r^4} \text{vec}[\mathbf{S}^2] \quad (19)$$

where three such equations are required for $j \in \{\text{x}, \text{y}, \text{z}\}$ and the derivatives of \mathbf{S} are derived algebraically from Eq. (16).

Since the directional derivatives of Eq. (17) and Eq. (18), together with time-propagators of Eq. (7), do not involve any matrix operations, other than a few trivial multiplications, ESCALADE offers substantial computational gains relative to the AUXMAT method in Eq. (14).

ACCELERATED NEWTON-RAPHSON OPTIMAL CONTROL

Moving away from a chosen calculation method of directional propagator derivatives, the remaining bottleneck of the Newton-Raphson methods presented above is the off-diagonal Hessian elements; the mixed derivatives of Eq. (13).

As a starting point, ESCALADE includes and additional efficiency, which also applies to the AUXMAT method, where the central effective propagator in Eq. (13) can be split to $\mathbf{U}_{m+1}^{n-1} = \mathbf{U}_{m+1}^{n-1} \mathbf{U}_1^n \mathbf{U}_m^1 = \mathbf{U}_1^{n-1} \mathbf{U}_m^1$, Eq. (13) becomes

$$\nabla^2 \mathcal{F}(c_{k,n}, c_{j,m}) = \text{Re} \langle \hat{\chi}_{n+1} D_{k,n} | \mathbf{U}_1^{n-1} \mathbf{U}_m^1 | D_{j,m} \hat{\rho}_{m-1} \rangle \quad (20)$$

An interpretation of these two central effective propagators is: the right hand side, $\langle \hat{\chi}_{n+1} D_{k,n} |$, is multiplied by the effective propagator \mathbf{U}_1^{n-1} , presenting the directional derivative of t_n to be evaluated at t_0 ; the left hand side, $| D_{j,m} \hat{\rho}_{m-1} \rangle$, is multiplied by the time-reversed effective propagator \mathbf{U}_m^1 , presenting the directional derivative of t_m to also be evaluated at t_0 .

To outline how this can be overcome, a representation of a *trajectory* is introduced:

$$[\rho]_m^n \triangleq [\hat{\rho}_n \rangle \hat{\rho}_{n-1} \rangle \dots \hat{\rho}_{m+1} \rangle \hat{\rho}_m] \quad (21)$$

which is an array of column vectors and the whole trajectory from the dynamics in Eq. (3) is contained in $[\rho_0^N]$. Trajectory analysis is useful for visualising pulse dynamics [50]. Taking the concept of a single matrix containing all trajectory information, a *directional derivative trajectory*, evaluated at t_0 as with the right side of Eq. (20), can be defined as

$$[\partial_j^{[0]} \rho]_0^n \triangleq [\mathbf{U}_n^1 D_{j,n} \hat{\rho}_{n-1} \rangle \dots \mathbf{U}_2^1 D_{j,2} \hat{\rho}_1 \rangle \mathbf{U}_1^\dagger D_{j,1} \hat{\rho}_0] \quad (22)$$

where the superscript $[0]$ is used to indicate evaluation at t_0 .

With the realisation that a *directional derivative trajectory* in Eq. (22) is a matrix in itself, n Hessian elements can be calculated with one matrix-vector product with

$$\begin{bmatrix} \nabla^2 \mathcal{F}(c_{k,n}, c_{j,n}) \\ \vdots \\ \nabla^2 \mathcal{F}(c_{k,n}, c_{j,2}) \\ \nabla^2 \mathcal{F}(c_{k,n}, c_{j,1}) \end{bmatrix}^T = \text{Re} \underbrace{\langle \hat{\chi}_{n+1} D_{k,n} \mathbf{U}_1^{n-1} |}_{N \text{ times backward}} \underbrace{[\partial_j^{[0]} \rho]_0^n}_{N \text{ times forward}} \quad (23)$$

Given that the total effective propagator \mathbf{U}_1^N can be calculated with forward propagation, \mathbf{U}_1^{n-1} can be updated during subsequent backward propagation with $\mathbf{U}_1^{n-1} = \hat{P}_{n-1}^\dagger \mathbf{U}_1^n$. The single vector-matrix product of Eq. (23), per time-slice, is expected to be much more efficient than the $n-1$ vector-vector products, per time-slice, in Eq. (13).

ACCELERATION OF A BROADBAND MRI EXAMPLE

The authors choose to set the test of the method presented above in the context of MRI because there is a very real need to

have computationally fast OC methods to run *on-the-fly* with a need for patient specific solutions. Often, OC-facilitated MRI exploits simultaneous/parallel control systems e.g. eight radiofrequency channels (x- and y-controls) [14, 51] and three magnetic field gradients and/or numerous local shims (z-controls) [40, 51, 52].

The optimisation is set as robust for an ensemble of 101 spin- $\frac{1}{2}$ systems, with offset bandwidth $\frac{\omega}{2\pi} \in [-\frac{1}{2}, +\frac{1}{2}]$ kHz, simulated using a single block-diagonal Liouvillian with each block operating on a single ensemble member [37, 41].

The time-slice, Δt , is often fixed to the hardware digitalisation dwell-time: typically a few μs . Modern MRI systems handle $N > 1000$, but the pulse duration, $T = N\Delta t$, is usually kept around a few ms to avoid degradation of pulse performance due to transverse relaxation. As a set of speed tests, these three variables are incremented and set as a range of OC problems and are shown in Fig. 2. The vertical dashed lines indicate a set of variables physically relevant to MRI.

Figure 2 shows the average speedup of the accelerated auxiliary matrix method (*acc-AUXMAT*) and the accelerated ESCALADE method (*acc-ESCALADE*), both relative to the standard auxiliary matrix method. A separate fidelity, gradient, and Hessian calculation is performed for each method from a random control waveform, with c_x , c_y , and c_z controls in the order of $2\pi \times 10^3 \text{ rad s}^{-1}$. The average is over 84 different random control pulses, run in parallel on 28 CPU cores.

Figure 2A shows that the effect of increasing T while also increasing Δt is, approximately, a constant speedup of *acc-AUXMAT* and *acc-ESCALADE* Hessian. This can be attributed to the effective propagator splitting of Eq. (20). The small speedup of *acc-AUXMAT* fidelity and gradient calculations is due to an algorithmic efficiency from coding in a way that lends itself to the accelerated Hessian methods.

The main result of this manuscript is the speedup of Hessian calculations of the *acc-AUXMAT* and *acc-ESCALADE* methods, with speedup increasing as N increases, in Fig. 2B and Fig. 2C, to over $\times 100$ when a large N is used. Furthermore, this trend does not appear to dampen, indicating further speedup when $N \gg 1000$.

From the evidence in Fig. 2B and Fig. 2C, the accelerated Hessian calculations of Eq. (23) do indeed remove the $\mathcal{O}(N^2)$ scaling of the original Newton-Raphson method [31], reducing to a linear scaling $\mathcal{O}(N)$.

CONCLUSION

A new mathematical formulation of the Newton-Raphson GRAPE method [31] has been presented in Liouville space and applies to optimal control problems with unitary evolution. The ESCALADE method [43] recast the cumbersome problem of finding derivatives – using trigonometric evaluations of vectorised arrays rather than matrix-matrix products and computationally expensive matrix exponentials – and factorised the central propagator to avoid $\mathcal{O}(N^2)$ scaling, now reduced to $\mathcal{O}(N)$, in the computation of the Hessian. The ES-

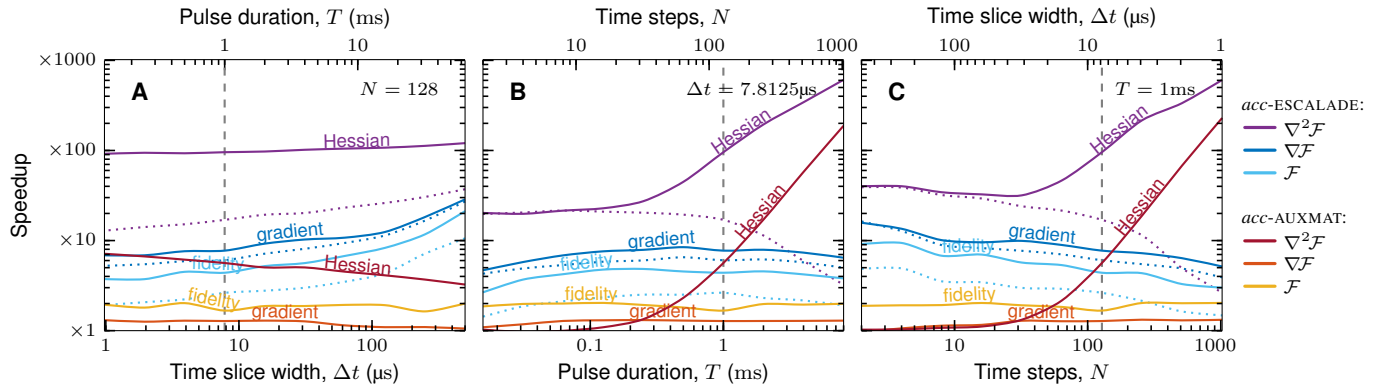


FIG. 2. The average speedup of the accelerated ESCALADE method (*acc*-ESCALADE) and the accelerated auxiliary matrix method (*acc*-AUXMAT), compared to the auxiliary matrix method. The number of time-steps, N , the time-slice width, Δt , and the pulse duration, T , are parameters affecting computation time. In each of the three plots one parameter is kept constant: (A) $N = 128$, (B) $\Delta t = 7.8125 \mu\text{s}$; and (C) $T = 1 \text{ ms}$. The dotted lines in each plot show the speedup of *acc*-ESCALADE relative to *acc*-AUXMAT.

CALADE method is shown in a new light of Liouville space, with the additional derivation of z-controls, which are important to MRI.

The main result is a new formulation of the Newton-Raphson GRAPE method in Liouville space, being an optimisation method with quadratic convergence to an optimal solution, reducing the expensive polynomial scaling of the control problem to a linear scaling when increasing the number of piecewise-constant pulses in optimal solution. Speedup increases as the number of time-slices, N , increases: $\times 4$ to $\times 200$, for $N = 100$ and $N = 1000$ respectively. Furthermore, employing ESCALADE within this new Hessian calculation method shows further speedup of $\times 70$ to $\times 600$, for $N = 100$ and $N = 1000$ respectively, when compared to the original Newton-Raphson GRAPE method.

DLG thanks Burkhard Luy for his continued support and Martin Goodwin for proofreading. MF wishes to thank the Royal Society for a University Research Fellowship and a University Research Fellow Enhancement Award (URF\R1\180233 and RGF\EA\181018). MSV would like to thank Villum Fonden, Eva og Henry Fraenckels Mindefond, Harboefonden, and Kong Christian Den Tiendes Fond.

080201 (2018).

- [3] J. C. Saywell, I. Kuprov, D. Goodwin, M. Carey, and T. Freegarde, Optimal control of mirror pulses for cold-atom interferometry, *Phys. Rev. A* **98**, 023625 (2018).
- [4] J. C. Saywell, *Optimal control of cold atoms for ultra-precise quantum sensors*, Ph.D. thesis, University of Southampton, UK (2020).
- [5] J. Saywell, M. Carey, M. Belal, I. Kuprov, and T. Freegarde, Optimal control of raman pulse sequences for atom interferometry, *J. Phys. B: At. Mol. Opt. Phys.* **53**, 085006 (2020).
- [6] J. Saywell, M. Carey, N. Dedes, I. Kuprov, and T. Freegarde, Can optimised pulses improve the sensitivity of atom interferometers?, in *Quantum Technology: Driving Commercialisation of an Enabling Science II*, Vol. 11881, edited by M. J. Padgett, K. Bongs, A. Fedrizzi, and A. Politi, International Society for Optics and Photonics (SPIE, 2021) pp. 83–92.
- [7] J. Zhang, R. Laflamme, and D. Suter, Experimental implementation of encoded logical qubit operations in a perfect quantum error correcting code, *Phys. Rev. Lett.* **109**, 100503 (2012).
- [8] G. Waldherr, Y. Wang, S. Zaiser, M. Jamali, T. Schulte-Herbrüggen, H. Abe, T. Ohshima, J. Isoya, J. F. Du, P. Neumann, and J. Wrachtrup, Quantum error correction in a solid-state hybrid spin register, *Nature* **506**, 204 (2014).
- [9] F. Dolde, V. Bergholm, Y. Wang, I. Jakobi, B. Naydenov, S. Pezzagna, J. Meijer, F. Jelezko, P. Neumann, T. Schulte-Herbrüggen, J. Biamonte, and J. Wrachtrup, High-fidelity spin entanglement using optimal control, *Nat. Commun.* **5**, 3371 (2014).
- [10] N. Khaneja, R. Brockett, and S. J. Glaser, Time optimal control in spin systems, *Phys. Rev. A* **63**, 032308 (2001).
- [11] T. E. Skinner, T. O. Reiss, B. Luy, N. Khaneja, and S. J. Glaser, Application of optimal control theory to the design of broadband excitation pulses for high-resolution NMR, *J. Magn. Reson.* **163**, 8 (2003).
- [12] N. Khaneja, T. Reiss, C. Kehlet, T. Schulte-Herbrüggen, and S. J. Glaser, Optimal control of coupled spin dynamics: design of NMR pulse sequences by gradient ascent algorithms, *J. Magn. Reson.* **172**, 296 (2005).
- [13] Z. Tošner, S. J. Glaser, N. Khaneja, and N. C. Nielsen, Effective Hamiltonians by optimal control: Solid-state NMR double-quantum planar and isotropic dipolar recoupling, *J. Chem. Phys.* **125**, 184502 (2006).

* david.goodwin@partner.kit.edu

† msv@cfin.au.dk

- [1] S. J. Glaser, U. Boscain, T. Calarco, C. P. Koch, W. Köckenberger, R. Kosloff, I. Kuprov, B. Luy, S. Schirmer, T. Schulte-Herbrüggen, D. Sugny, and F. K. Wilhelm, Training schrödinger's cat: quantum optimal control, *Eur. Phys. J. D* **69**, 279 (2015).
- [2] A. Acín, I. Bloch, H. Buhrman, T. Calarco, C. Eichler, J. Eisert, D. Esteve, N. Gisin, S. J. Glaser, F. Jelezko, S. Kuhr, M. Lewenstein, M. F. Riedel, P. O. Schmidt, R. Thew, A. Wallraff, I. Walmsley, and F. K. Wilhelm, The quantum technologies roadmap: a european community view, *New J. Phys.* **20**,

[14] M. S. Vinding, D. Brenner, D. H. Y. Tse, S. Vellmer, T. Vosegaard, D. Suter, T. Stöcker, and I. I. Maximov, Application of the limited-memory quasi-Newton algorithm for multi-dimensional, large flip-angle RF pulses at 7T, *Magn. Reson. Mater. Phys.* **30**, 29 (2017).

[15] E. V. Reeth, H. Ratiney, K. Tse Ve Koon, M. Tesch, D. Grenier, O. Beuf, S. J. Glaser, and D. Sugny, A simplified framework to optimize MRI contrast preparation, *Magn. Reson. Med.* **81**, 424 (2019).

[16] J. Somlói, V. A. Kazakov, and D. J. Tannor, Controlled dissociation of I_2 via optical transitions between the X and B electronic states, *Chem. Phys.* **172**, 85 (1993).

[17] W. Zhu, J. Botina, and H. Rabitz, Rapidly convergent iteration methods for quantum optimal control of population, *J. Chem. Phys.* **108**, 1953 (1998).

[18] Y. Maday and G. Turinici, New formulations of monotonically convergent quantum control algorithms, *J. Chem. Phys.* **118**, 8191– (2003).

[19] R. Eitan, M. Mundt, and D. J. Tannor, Optimal control with accelerated convergence: Combining the Krotov and quasi-Newton methods, *Phys. Rev. A* **83**, 053426 (2011).

[20] P. Doria, T. Calarco, and S. Montangero, Optimal control technique for many-body quantum dynamics, *Phys. Rev. Lett.* **106**, 190501 (2011).

[21] N. Rach, M. M. Müller, T. Calarco, and S. Montangero, Dressing the chopped-random-basis optimization: A bandwidth-limited access to the trap-free landscape, *Phys. Rev. A* **92**, 062343 (2015).

[22] G. Ciaramella, A. Borzì, G. Dirr, and D. Wachsmuth, Newton methods for the optimal control of closed quantum spin systems, *SIAM J. Sci. Comput.* **37**, A319 (2015).

[23] S. Machnes, E. Assémat, D. Tannor, and F. K. Wilhelm, Tunable, flexible, and efficient optimization of control pulses for practical qubits, *Phys. Rev. Lett.* **120**, 150401 (2018).

[24] D. Lucarelli, Quantum optimal control via gradient ascent in function space and the time-bandwidth quantum speed limit, *Phys. Rev. A* **97**, 062346 (2018).

[25] D. Quiñones Valles, S. Dolgov, and D. Savostyanov, Tensor product approach to quantum control, in *Integral Methods in Science and Engineering: Analytic Treatment and Numerical Approximations*, edited by C. Constanda and P. Harris (Springer, 2019) pp. 367–379.

[26] S. Conolly, D. Nishimura, and M. A., Optimal control solutions to the magnetic resonance selective excitation problem, *IEEE Trans. Med. Imaging* **5**, 106 (1986).

[27] J. Mao, T. H. Mareci, K. N. Scott, and E. R. Andrew, Selective inversion radiofrequency pulses by optimal control, *J. Magn. Reson.* **70**, 310 (1986).

[28] L. Viola and S. Lloyd, Dynamical suppression of decoherence in two-state quantum systems, *Phys. Rev. A* **58**, 2733 (1998).

[29] L. Viola, E. Knill, and S. Lloyd, Dynamical decoupling of open quantum systems, *Phys. Rev. Lett.* **82**, 2417 (1999).

[30] P. de Fouquieres, S. G. Schirmer, S. J. Glaser, and I. Kuprov, Second order gradient ascent pulse engineering, *J. Magn. Reson.* **212**, 412 (2011).

[31] D. L. Goodwin and I. Kuprov, Modified Newton-Raphson GRAPE methods for optimal control of spin systems, *J. Chem. Phys.* **144**, 204107 (2016).

[32] A. N. Pechen and D. J. Tannor, Are there traps in quantum control landscapes?, *Phys. Rev. Lett.* **106**, 120402 (2011).

[33] K. Kobzar, T. E. Skinner, N. Khaneja, S. J. Glaser, and B. Luy, Exploring the limits of broadband excitation and inversion pulses, *J. Magn. Reson.* **170**, 236 (2004).

[34] K. Kobzar, T. E. Skinner, N. Khaneja, S. J. Glaser, and B. Luy, Exploring the limits of broadband excitation and inversion: II. Rf-power optimized pulses, *J. Magn. Reson.* **194**, 58 (2008).

[35] D. L. Goodwin, *Advanced optimal control methods for spin systems*, Ph.D. thesis, University of Southampton, UK (2017).

[36] Z. Tošner, M. J. Brandl, J. Blahut, S. J. Glaser, and B. Reif, Maximizing efficiency of dipolar recoupling in solid-state NMR using optimal control sequences, *Sci. Adv.* **7**, eabj5913 (2021).

[37] I. Kuprov, Fokker-Planck formalism in magnetic resonance simulations, *J. Magn. Reson.* **270**, 124 (2016).

[38] M. S. Vinding, B. Skyum, R. Sangill, and T. E. Lund, Ultrafast (milliseconds), multidimensional RF pulse design with deep learning, *Magn. Reson. Med.* **82**, 586 (2019).

[39] M. S. Vinding, C. S. Aigner, S. Schmitter, and T. E. Lund, DeepControl: 2DRF pulses facilitating inhomogeneity and B_0 off-resonance compensation in vivo at 7T, *Magn. Reson. Med.* **85**, 3308 (2021).

[40] M. S. Vinding, D. L. Goodwin, I. Kuprov, and T. E. Lund, Optimal control gradient precision trade-offs: Application to fast generation of DeepControl libraries for MRI, *J. Magn. Reson.* **333**, 107094 (2021).

[41] D. L. Goodwin, M. R. M. Koos, and B. Luy, Second order phase dispersion by optimised rotation pulses, *Phys. Rev. Research* **2**, 033157 (2020).

[42] M. F. Dempsey, B. Condon, and D. M. Hadley, MRI safety review, in *Seminars in Ultrasound, CT and MRI*, Vol. 23 (2002) pp. 392–401.

[43] M. Foroozandeh and P. Singh, Optimal control of spins by analytical Lie algebraic derivatives, *Automatica* **129**, 109611 (2021).

[44] W. Kallies, *Concurrent optimization of robust refocused pulse sequences for magnetic resonance spectroscopy*, Ph.D. thesis, Technische Universität München, DE (2018).

[45] D. L. Goodwin and I. Kuprov, Auxiliary matrix formalism for interaction representation transformations, optimal control, and spin relaxation theories, *J. Chem. Phys.* **143**, 084113 (2015).

[46] D. J. Siminovitch, Rotations in NMR: Part I. Euler-Rodrigues parameters and quaternions, *Concepts Magn. Reson.* **9**, 149 (1997).

[47] S. J. Glaser, T. Schulte-Herbrüggen, M. Sieveking, O. Schedletzky, N. C. Nielsen, O. W. Sørensen, and C. Griesinger, Unitary control in quantum ensembles: Maximizing signal intensity in coherent spectroscopy, *Science* **280**, 421 (1998).

[48] C. F. Van Loan, Computing integrals involving the matrix exponential, *IEEE Trans. Automat. Contr.* **23**, 395 (1978).

[49] D. L. Goodwin, P. Singh, and M. Foroozandeh, Adaptive optimal control of entangled qubits (2022), accepted for publication in *Sci. Adv.*

[50] I. Kuprov, Spin system trajectory analysis under optimal control pulses, *J. Mag. Reson.* **233**, 107 (2013).

[51] M. Vinding, B. Guérin, T. Vosegaard, and N. Nielsen, Local SAR, global SAR, and power-constrained large-flip-angle pulses with optimal control and virtual observation points, *Magnetic Resonance in Medicine* **77**, 374 (2017).

[52] J. P. Stockmann and L. L. Wald, In vivo B_0 field shimming methods for MRI at 7 T, *NeuroImage* **168**, 71 (2018).